Frequency- and temperature-dependent dielectric response in hybrid molecular beam epitaxy-grown BaSnO3 films

Nunn, William ; Prakash, Abhinav ; Bhowmik, Arghya; Haislmaier, Ryan ; Yue, Jin; García Lastra, Juan Maria; Jalan, Bharat

Published in:
A P L Materials

Link to article, DOI:
10.1063/1.5027567

Publication date:
2018

Document Version
Publisher's PDF, also known as Version of record

Frequency- and temperature-dependent dielectric response in hybrid molecular beam epitaxy-grown $BaSnO_3$ films

William Nunn, Abhinav Prakash, Arghya Bhowmik, Ryan Haislmaier, Jin Yue, Juan Maria Garcia Lastra, and Bharat Jalan

Citation: APL Materials **6**, 066107 (2018); doi: 10.1063/1.5027567
View online: https://doi.org/10.1063/1.5027567
View Table of Contents: http://aip.scitation.org/toc/apm/6/6
Published by the American Institute of Physics

Frequency- and temperature-dependent dielectric response in hybrid molecular beam epitaxy-grown $BaSnO_3$ films

William Nunn,[1] Abhinav Prakash,[1] Arghya Bhowmik,[2] Ryan Haislmaier,[1] Jin Yue,[1] Juan Maria Garcia Lastra,[2] and Bharat Jalan[1,a]
[1]*Department of Chemical Engineering and Materials Science, University of Minnesota, Minneapolis, Minnesota 55455, USA*
[2]*Department of Energy Conversion and Storage, Technical University of Denmark, Lyngby, Denmark*

(Received 3 March 2018; accepted 1 June 2018; published online 15 June 2018)

We report on the dielectric response of epitaxial $BaSnO_3$ films grown on Nb-doped $SrTiO_3$ (001) substrates using a hybrid molecular beam epitaxy approach. Metal-insulator-metal capacitors were fabricated to obtain frequency- and temperature-dependent dielectric constant and loss. Irrespective of film thickness and cation stoichiometry, the dielectric constant obtained from $Ba_{1-x}Sn_{1-y}O_3$ films remained largely unchanged at 15-17 and was independent of frequency and temperature. A loss tangent of $\sim 1 \times 10^{-3}$ at 1 kHz $< f <$ 100 kHz was obtained for stoichiometric films, which increased significantly with non-stoichiometry. Using density functional theory calculations, these results are discussed in the context of point defect complexes that can form during film synthesis. https://doi.org/10.1063/1.5027567

$BaSnO_3$ (BSO) is a wide bandgap perovskite oxide, which has recently gained considerable attention due to the discovery of a large room temperature mobility.[1–9] When doped with La, BSO has been shown to have a mobility of 320 $cm^2\ V^{-1}\ s^{-1}$ in bulk[5–7] and up to 183 $cm^2\ V^{-1}\ s^{-1}$ in thin films at remarkably high carrier densities of the order of 10^{20} cm^{-3}.[4] The combination of high carrier density and mobility makes doped BSO a promising candidate for transparent conducting oxides and power electronic applications.[10–12] Both electronic and optical properties of BSO can be strongly affected by their dielectric behavior. However, despite the increasing amount of work on the electronic and optical properties of BSO, there have been no reports on the dielectric response of BSO in thin film form. A few reports of dielectric properties exist and are measured using polycrystalline bulk samples.[13–16] For example, a dielectric constant of about 20 is reported for bulk BSO ceramics synthesized using a solid state ceramic method.[13] Most recent work reported a value of 45 using powder BSO samples.[16] Theoretical calculations have also been carried out and have predicted a value of 22, which is in good agreement with the experimental bulk value.[16]

Thin film geometry can offer additional advantages of tailoring dielectric constant through strain engineering approaches. However, it also yields several challenges associated with point defect control and strain relaxation-induced dislocation formation. The latter becomes a more severe problem for films that have large lattice mismatch with substrates, as is commonly the case with BSO.[3,4,17–19] A large density of threading dislocations, 10^{11}-10^{12} cm^{-2}, is nominally found in BSO films grown on various substrates including $SrTiO_3$ (STO) (001).[4,18,20] These dislocations are argued to be charged centers[2,6,21] can arguably influence polarization and thereby dielectric constant of BSO in thin film geometry. Additionally, factors such as film/electrode interfaces can influence the dielectric constant of BSO films. For instance, thickness-dependent dielectric constants have been commonly observed in ferroelectric systems including the (Ba, Sr)TiO_3 (BSTO) system owing to an interfacial "dead layer" effect.[22–25] It is, however, also argued that the dead layer effect may not be observable in films having a low dielectric constant.[26]

[a]Author to whom correspondence should be addressed: bjalan@umn.edu

In this letter, we report on the dielectric constant (ε') and the dielectric loss tangent ($\tan\delta$) of nominally stoichiometric BSO films as a function of film thickness, frequency, and temperature between 77 and 300 K. Films grown under Ba- and Sn-deficient conditions are also examined to investigate the role of cation stoichiometry on dielectric responses. These results are then discussed using density functional theory (DFT) calculations revealing the important role of Ba, Sn, and O vacancies and related defect complexes on the dielectric constant of BSO.

BSO films were grown on conducting 0.5 wt. % Nb-doped $SrTiO_3$ (001) (NSTO) substrates using a hybrid molecular beam epitaxy (MBE) approach described elsewhere.[2,19,21] NSTO was used as a bottom metal electrode and has a room temperature resistivity of $\sim 5 \times 10^{-3}$ Ω cm. Stoichiometry was tailored by controlling Sn:Ba beam equivalent pressure (BEP) ratios.[21] The degree of non-stoichiometry was estimated by correlating Sn:Ba BEPs and the BSO out-of-plane lattice parameters with the Rutherford Backscattering spectrometry (RBS) results for BSO films grown on $SrTiO_3$.[21] The metal-insulator-metal (MIM) capacitor structures, as illustrated schematically in the inset of Fig. 1, were fabricated for dielectric measurements by sputtering 200 nm of Pt on BSO films and using a lift-off technique to make top electrodes with radii of 100 μm. An outer ring of the BSO films was then etched through to the substrate/bottom electrode using ion milling. The samples were annealed at 900 °C for 1 h in excess of oxygen to decrease possible contributions from oxygen vacancies that may be introduced during the ion milling process. It is noted that as-grown BSO films were insulating suggesting no measurable oxygen vacancy defects. Finally, 20 nm Al/30 nm Ni/150 nm Au was sputtered on the outer ring to create an ohmic contact with substrate.

Wide-angle x-ray diffraction (WAXRD) 2θ-ω scans were taken on a Panalytical X'Pert thin film diffractometer. Complex impedances were measured using an Agilent B1500A from 1 kHz to 1 MHz with a peak oscillating electric field of about 20 kV/cm. A Lakeshore CPX-VF cryogenic probe station was used to perform temperature-dependent impedance measurements from 77 to 300 K. A variety of defect states within a $2 \times 2 \times 2$ supercell were studied using DFT-based simulations for formation energy and dielectric properties. The methodology and detailed results of chosen configurations that are likely to exist in our samples are provided in the supplementary material.

Figure 1 shows the WAXRD pattern of the film stack in a MIM capacitor configuration consisting of 40 nm stoichiometric BSO/NSTO (001) and metal electrodes after complete processing. A schematic of the capacitor structure is shown in the inset. The WAXRD result shows phase-pure, epitaxial, single crystalline BSO films on NSTO (001). Additional peaks corresponding to Pt (111) and Au (111) were also present indicating crystalline and textured metal electrodes. It is noted that cation

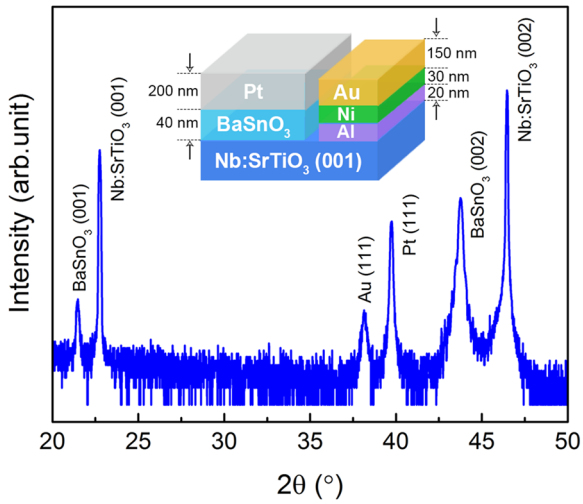

FIG. 1. High-resolution WAXRD pattern for a 40 nm BSO film on Nb-doped $SrTiO_3$ (001) substrate after complete capacitor fabrication. Inset shows a schematic of the device structure.

stoichiometry and epitaxial relationship for BSO films were confirmed using adsorption-controlled growth regime offered by the hybrid MBE approach.[19,21]

Figures 2(a) and 2(b) show the frequency (f) dependence of ε' and $\tan\delta$, respectively, for films with different compositions. Film thicknesses were kept between 40 and 49 nm. Fits in Fig. 2(b) for $\tan\delta$ as a function of f were calculated from complex impedance fits using the equivalent circuit shown as an inset. Best fits were found using a constant phase element (CPE_f) for the film, which may act as an imperfect capacitor. The overall impedance (Z) of the circuit is therefore given by

$$Z = R_{el} + \left(\frac{R_f}{1 + R_f Q(j\omega)^{\alpha}}\right) + j\omega L, \tag{1}$$

where R_{el} and R_f are the electrode and film resistance, respectively; $\omega = 2\pi f$, Q is a frequency-independent constant, and L is the inductance of the equivalent circuit. α is a parameter between 0 and 1 which gives the constant phase of $-(90\alpha)°$, where $\alpha = 1$ is a perfect capacitor and $\alpha = 0$ is a pure resistor. Regardless of stoichiometry, excellent fits were obtained using this circuit and yielded $\alpha = 0.998$–0.999, further confirming nearly perfect capacitor behavior. An inductance of 5.5 μH was also found from the fit, which is in good agreement with perovskite thin film capacitors and has usually been attributed to the electrode behavior.[27] The frequency-dependent value of ε' remained largely unchanged for all samples [see Fig. 2(a)]. A value of 14.8 ± 0.5 was measured for stoichiometric (Sn:Ba = 1.00 ± 0.02) and Ba-deficient (Sn:Ba = 1.15 ± 0.02) films, whereas a slightly higher value, 15.6 ± 0.5, was obtained for Sn-deficient film (Sn:Ba = 0.95 ± 0.02). Stoichiometric films, however, yielded much lower $\tan\delta$, $1.6 \times 10^{-3} \pm 1 \times 10^{-4}$ in 1 kHz $< f <$ 100 kHz, whereas much higher $\tan\delta$ was obtained for non-stoichiometric films, likely due to cation vacancy defects or defect complexes. Irrespective of cation stoichiometry, all three samples showed an increase in $\tan\delta$ for $f >$ 100 kHz, suggesting an onset of dielectric relaxation. A larger frequency range would be needed to confirm dielectric relaxation processes in BSO films.

Our experimental results for thin BSO films have about a 25% lower dielectric constant than the reported bulk value of 20 in ceramic samples, and these values are independent of cation stoichiometry. These findings raised questions on the possible roles of dimensionality, threading dislocations, and interfaces that may degrade a film's dielectric performance. To this end, we grew a thickness series of nominally stoichiometric BSO films to determine how dielectric properties evolve with film thickness (t). Figures 2(c) and 2(d) show ε' and $\tan\delta$, respectively, measured at f = 100 kHz

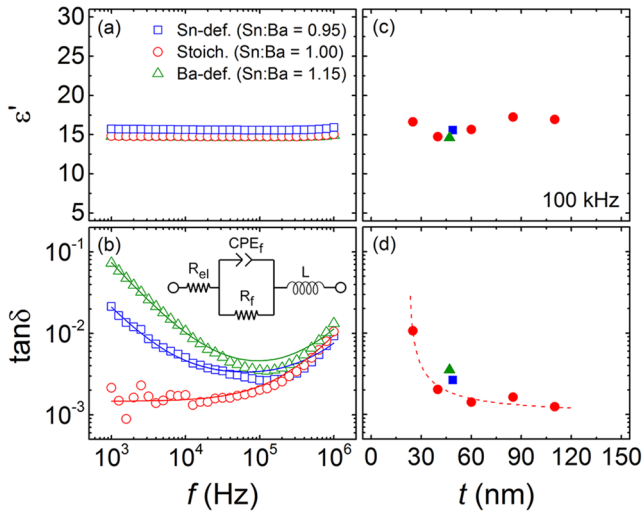

FIG. 2. Frequency dependence of (a) ε' and (b) $\tan\delta$ for stoichiometric (40 nm), Sn-deficient (49 nm), and Ba-deficient (47 nm) BSO films. Error to the RBS composition is ±0.02. Solid lines are fits using the schematic equivalent circuit as illustrated in the inset incorporating electrode (R_{el}) and film (R_f) resistance, film capacitance in terms of a constant phase element (CPE_f), and inductance (L). Film thickness dependence of (c) ε' and (d) $\tan\delta$ for stoichiometric and Ba- and Sn-deficient films measured at 100 kHz. Dashed line is a guide to the eye. Error bars are of the size of symbols.

for stoichiometric films (red circles). Results of Ba-deficient (green triangle) and Sn-deficient (blue square) samples are also shown on the same plots for comparison. ε′ was found to be relatively constant, whereas tan δ decreased hyperbolically with increasing film thickness to a value ~1×10^{-3}. A similar behavior of tan δ vs f was seen by Li *et al.*[28] for $SrTiO_3$ films and was attributed to the interfacial "dead layer" effect. However, it is noteworthy that there was no change in ε′ vs t as one may expect from a dead layer. We attribute this behavior to the low dielectric constant of BSO, which may not allow for the direct observation of a dead layer effect through ε′ vs t even if a dead layer is present.[26] Another factor that may influence the dielectric loss is threading dislocation density in BSO films. In our prior work, we have found evidence that threading dislocation density decreases with increasing thicknesses resulting in an increase of electron mobility.[2] While dislocation density is yet to be measured experimentally, it is conceivable to attribute the observed behavior of tan δ vs f to the threading dislocations. Future theoretical work should be directed to investigate the role of dielectric dead layer and threading dislocations on dielectric loss.

Finally, we investigated the temperature dependence of dielectric constant and loss. Figures 3(a) and 3(b) show T-dependent ε′ and tan δ, respectively, measured at 100 kHz from 77 to 300 K for films with different cation stoichiometry. No change in ε′ was observed in this temperature range, but tan δ showed significant variation with temperature. With decreasing temperature, tan δ first increased for the stoichiometric sample followed by a broad peak around 100-175 K. A similar broad peak was observed for Ba-deficient films, but tan δ initially decreased with decreasing temperature. Sn-deficient films, on the other hand, showed a drop in tan δ with decreasing temperature reaching below that of stoichiometric film and no obvious broad peak. While it is yet to be established the main source of peak in tan δ, we attribute it to extrinsic defects[29] including threading dislocations, residual oxygen

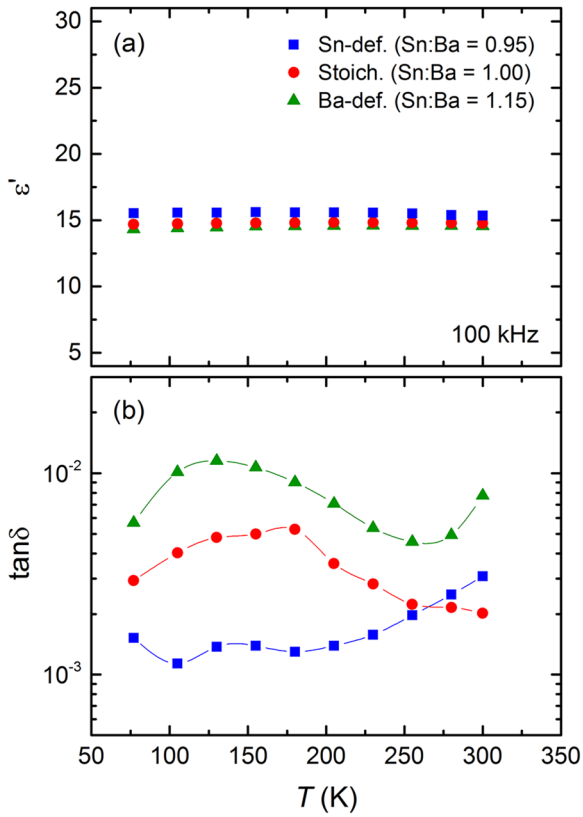

FIG. 3. Temperature dependence of (a) ε′ and (b) tan δ measured at 100 kHz for stoichiometric (40 nm), Sn-deficient (49 nm), and Ba-deficient (47 nm) BSO films. Error to the RBS composition is ±0.02, and error bars are of the size of symbols.

vacancies,[30] or phase transition in the NSTO substrate. Intrinsic factors such as Debye dielectric loss can also result in a peak in tan δ with temperature, but this behavior is usually operative at much higher frequencies. The true source of the observed loss behavior is still unknown, and further work is necessary to determine its source.

To investigate an apparent tolerance of the dielectric constant to cation stoichiometry, DFT simulations were used. The calculated dielectric constant for bulk, defect-free BSO, was 18.1 comprising electronic and ionic contributions of 4.7 and 13.4, respectively. The calculated electronic contribution agrees well with previous theoretical work by Bévillon *et al.*,[16] whereas the ionic contribution is smaller. The discrepancy arises from the difference in phonon frequency estimates, although Born charges (Z^*_{xx} of +2.76/+0.37/−3.34 for Ba/Sn/O ions) match with the reported values.[16] To simulate defect structures in non-stoichiometric films, a subset of possible defect configurations including cation and oxygen vacancies and their defect complexes were considered. DFT yielded formation energies of +0.71 eV for $\ddot{V}_o$ and +6.22 eV and +10.66 eV for V''_{Ba} and V''''_{Sn}, respectively. A possible defect complex in Sn-deficient samples consisting of one V''''_{Sn} and two $\ddot{V}_o$ in the 40 atom supercell showed a total vacancy formation energy of +3.88 eV when these vacancies are next to each other, i.e., $\ddot{V}_o - V''''_{Sn} - \ddot{V}_o$ angle is 90° (supplementary material). Similarly, for a Ba-deficient sample, a defect complex consisting of one V''_{Ba} and one $\ddot{V}_o$ vacancy requires much lower formation energy, +3.67 eV, when there is a missing O atom in the second coordination, 5.03 Å from missing the Ba atom (supplementary material). The Born effective charge tensor, a second order derivative of the total energy with respect to macroscopic electric field and atomic displacement, indicates the significance of long-range Coulomb interactions on the vibrational and optical properties of ionic insulators. For different supercell configurations with these two vacancy complexes, DFT calculation revealed small changes in the Born charge of ions. Low frequency phonon modes have the largest contributions to the dielectric response and our calculations point to no significant modification in their frequencies. This leads to a very small reduction in the ionic contribution to the dielectric constant (see the supplementary material). Similarly, the electronic contribution to the dielectric constant remained largely unchanged. The very small changes in the Born charge and resulting dielectric constant of these non-stoichiometry related defect complexes, therefore, agrees well with the experimental findings of no measurable influence on dielectric constant with non-stoichiometry.

In summary, we have characterized dielectric properties of BSO films grown by hybrid MBE. The measured dielectric constant was 15-17 for stoichiometric films and remained largely unchanged with stoichiometry, film thickness, frequency, and temperature. Stoichiometric films yielded the lowest tan δ, 1×10^{-3} at room temperature, but exhibited a broad peak between 100 and 175 K. DFT simulations were used to investigate the effect of possible point defects/defect complexes on the dielectric constant and was found to be consistent with our experimental results. Future theoretical work should, however, be directed to investigate the specific contribution of different defects on dielectric loss behavior.

See supplementary material for possible defect configurations chosen for density functional theory calculations in addition to the high resolution XRD and temperature-dependent dielectric loss data at different frequencies.

The authors thank Richard D. James, Hanlin Gu, and Nini Pryds for helpful discussion. W.N. thanks Matt Robbins for help with impedance measurements and training. This work was primarily supported by the National Science Foundation through No. DMR-1741801 and partially by the UMN MRSEC program under Award No. DMR-1420013. A part of this work was supported through the Young Investigator Program of the Air Force Office of Scientific Research (AFOSR) through Grant No. FA9550-16-1-0205. The work also acknowledges partial support from the RDF Fund of the Institute on the Environment (UMN). Parts of this work were carried out at the Minnesota Nano Center and Characterization Facility, University of Minnesota, which receives partial support from NSF through the MRSEC program. A.P. would like to acknowledge the support from the UMN Doctoral Dissertation Fellowship. For DFT work, J.M.G.L. acknowledges funding support from the Villum Foundation's Young Investigator Programme through the Mat4Bat project (Grant No. 10096).

[1] S. I. Beigi, F. J. Walker, S. W. Cheong, K. M. Rabe, and C. H. Ahn, APL Mater. **3**, 062510 (2015).
[2] A. Prakash, P. Xu, A. Faghaninia, S. Shukla, J. W. Ager III, C. S. Lo, and B. Jalan, Nat. Commun. **8**, 15167 (2017).
[3] S. Raghavan, T. Schumann, H. Kim, J. Y. Zhang, T. A. Cain, and S. Stemmer, APL Mater. **4**, 016106 (2016).
[4] H. Paik, Z. Chen, E. Lochocki, A. Seidner H., A. Verma, N. Tanen, J. Park, M. Uchida, S. Shang, B.-C. Zhou, M. Brützam, R. Uecker, Z.-K. Liu, D. Jena, K. M. Shen, D. A. Muller, and D. G. Schlom, APL Mater. **5**, 116107 (2017).
[5] H. J. Kim, U. Kim, H. M. Kim, T. H. Kim, H. S. Mun, B.-G. Jeon, K. T. Hong, W.-J. Lee, C. Ju, K. H. Kim, and K. Char, Appl. Phys. Express **5**, 061102 (2012).
[6] H. J. Kim, U. Kim, T. H. Kim, J. Kim, H. M. Kim, B.-G. Jeon, W.-J. Lee, H. S. Mun, K. T. Hong, J. Yu, K. Char, and K. H. Kim, Phys. Rev. B **86**, 165205 (2012).
[7] X. Luo, Y. S. Oh, A. Sirenko, P. Gao, T. A. Tyson, K. Char, and S.-W. Cheong, Appl. Phys. Lett. **100**, 172112 (2012).
[8] A. V. Sanchela, T. Onozato, B. Feng, Y. Ikuhara, and H. Ohta, Phys. Rev. Mater. **1**, 034603 (2017).
[9] K. Ganguly, A. Prakash, B. Jalan, and C. Leighton, APL Mater. **5**, 056102 (2017).
[10] K. Krishnaswamy, L. Bjaalie, B. Himmetoglu, A. Janotti, L. Gordon, and C. G. Van de Walle, Appl. Phys. Lett. **108**, 083501 (2016).
[11] S. A. Chambers, T. C. Kaspar, A. Prakash, G. Haugstad, and B. Jalan, Appl. Phys. Lett. **108**, 152104 (2016).
[12] C. Park, U. Kim, C. J. Ju, J. S. Park, Y. M. Kim, and K. Char, Appl. Phys. Lett. **105**, 203503 (2014).
[13] P. Singh, B. J. Brandenburg, C. P. Sebastian, P. Singh, S. Singh, D. Kumar, and O. Parkash, Jpn. J. Appl. Phys., Part 1 **47**, 3540 (2008).
[14] S. Upadhyay, O. Parkash, and D. Kumar, J. Mater. Sci. Lett. **16**, 1330 (1997).
[15] S. Upadhyay, Bull. Mater. Sci. **36**, 1019 (2013).
[16] É. Bévillon, A. Chesnaud, Y. Wang, G. Dezanneau, and G. Geneste, J. Phys.: Condens. Matter **20**, 145217 (2008).
[17] K. Ganguly, P. Ambwani, P. Xu, J. S. Jeong, K. A. Mkhoyan, C. Leighton, and B. Jalan, APL Mater. **3**, 062509 (2015).
[18] H. Mun, U. Kim, H. M. Kim, C. Park, T. H. Kim, H. J. Kim, K. H. Kim, and K. Char, Appl. Phys. Lett. **102**, 252105 (2013).
[19] A. Prakash, J. Dewey, H. Yun, J. S. Jeong, K. A. Mkhoyan, and B. Jalan, J. Vac. Sci. Technol., A **33**(6), 060608 (2015).
[20] W. Y. Wang, Y. L. Tang, Y. L. Zhu, J. Suriyaprakash, Y. B. Xu, Y. Liu, B. Gao, S.-W. Cheong, and X. L. Ma, Sci. Rep. **5**, 16097 (2015).
[21] A. Prakash, P. Xu, X. Wu, G. Haugstad, X. Wang, and B. Jalan, J. Mater. Chem. C **5**, 5730 (2017).
[22] C. S. Hwang, J. Appl. Phys. **92**, 432 (2002).
[23] S. Yamamichi, H. Yabuta, T. Sakuma, and Y. Miyasaka, Appl. Phys. Lett. **64**, 1644 (1994).
[24] T. Horikawa, N. Mikami, T. Makita, J. Tanimura, M. Kataoka, K. Sato, and M. Nunoshita, Jpn. J. Appl. Phys., Part 1 **32**, 4126 (1993).
[25] C. B. Parker, J.-P. Maria, and A. I. Kingon, Appl. Phys. Lett. **81**, 340 (2002).
[26] K. Natori, D. Otani, and N. Sano, Appl. Phys. Lett. **73**, 632 (1998).
[27] M. S. Tsai and T. Y. Tseng, Mater. Chem. Phys. **57**, 47 (1998).
[28] H.-C. Li, W. Si, A. D. West, and X. Xi, Appl. Phys. Lett. **73**, 464 (1998).
[29] V. V. Laguta, M. D. Glinchuk, I. P. Bykov, J. Rosa, L. Jastrabik, M. Savinov, and Z. Trybuła, Phys. Rev. B **61**, 3897 (2000).
[30] Z. Yu, C. Ang, and L. Cross, Appl. Phys. Lett. **74**, 3044 (1999).